Available online at www.sciencedirect.com
ScienceDirect
Journal of Solid State Chemistry 181 (2008) 515–524
JOURNAL OF SOLID STATE CHEMISTRY
www.elsevier.com/locate/jssc

The effect of replacement of Sr by Ca on the structural and luminescence properties of the red-emitting $Sr_2Si_5N_8:Eu^{2+}$ LED conversion phosphor

Y.Q. Li, G. de With, H.T. Hintzen*

Department of Chemical Engineering and Chemistry, Eindhoven University of Technology, P.O. Box 513, 5600 MB Eindhoven, The Netherlands

Received 10 July 2007; received in revised form 1 November 2007; accepted 15 November 2007
Available online 15 December 2007

Abstract

The influence of the replacement of Sr by Ca on structural and luminescence properties of Eu^{2+}-doped $Sr_2Si_5N_8$ is reported. The Rietveld refinement of the powder X-ray diffraction data shows that the Ca^{2+} ion preferentially occupies the larger Sr site in $Sr_2Si_5N_8:Eu^{2+}$. Although the excitation spectrum is hardly modified, the position of the emission band of Eu^{2+} can be tailored through partial replacement of Sr by Ca in $Sr_2Si_5N_8:Eu^{2+}$, resulting in red-emission shifting from 620 to 643 nm. Furthermore, $(Sr, Ca)_2Si_5N_8:Eu^{2+}$ shows high potential as a conversion phosphor for white-light LED applications due to similar absorption, conversion efficiency and thermal quenching behaviour for 465 nm excitation after the introduction of the Ca ion.

Keywords: Luminescence; Phosphor; Alkaline-earth-silicon-nitride; Calcium; Strontium; Europium; X-ray powder diffraction; Rietveld refinement; White-light LEDs

1. Introduction

Red-emitting $M_2Si_5N_8:Eu^{2+}$ ($M = Ca, Sr, Ba$) phosphors are attracting extensive attention due to its excellent performance for white-LED lighting applications [1–6]. Moreover, $Sr_2Si_5N_8:Eu^{2+}$ shows the best thermal quenching behaviour among $M_2Si_5N_8:Eu^{2+}$ ($M = Ca, Sr, Ba$) phosphors [3]. In general, $M_2Si_5N_8:Eu^{2+}$ ($M = Ca, Sr, Ba$) shows unusual long-wavelength broadband emission between 575 and 680 nm depending on the type of the M ion and the Eu concentration [1–3,6]. It can be efficiently excited from the near UV to blue range (370–465 nm) and in this way convert absorbed UV–blue radiation from the InGaN-based LED to orange–red light. The long-wavelength emission is attributed to a high covalency of the host-lattice and a large crystal-field splitting effect on the Eu^{2+} 5*d* band due to the presence of coordinating nitrogen [3,7,8]. When excited by 465 nm, the conversion (quantum) efficiency is higher for $M = Sr, Ba$ (~75–80%) than for $M = Ca$ (~35–40%) [3]. As conversion phosphors for use in white-light LEDs, a high chemical, thermal and radiation stability is necessary for achieving long lifetime of the devices [9]. With the ionic radius of M increasing going from Ca to Ba, the alkaline-earth compound generally tends to become less stable towards O_2, H_2O and CO_2 as well as elevated temperatures. As an evidence of this, the sensitivity towards oxidation of $M_2Si_5N_8:Eu^{2+}$ ($M = Ca, Sr, Ba$) exposed to air at 300–600 °C increases in the sequence of $Ca < Sr < Ba$ [2]. Therefore, partial replacement of Sr by Ca in $M_2Si_5N_8:Eu^{2+}$ ($M = Sr, Ba$) is expected to further improve the stability, as also found for $Sr_{1-x}Ca_xS:Eu^{2+}$ [7]. In addition, it is well established that the luminescence properties can be tuned by not only the Eu concentration but also by partial cross-substitution between alkaline-earth ions, for example replacement of Sr by Ca and/or Ba [10–13]. There are two crystallographic M sites present in the $M_2Si_5N_8$ lattice, thus better understanding of whether or not Ca and Eu ions have site preference in the $Sr_2Si_5N_8$ lattice is valuable for further improvement of the performance of $Sr_2Si_5N_8:Eu^{2+}$ phosphors from both the practical and scientific point of views. In this paper, therefore, the focus is on the investigation of the effect of the substitution of Ca for Sr in $Sr_2Si_5N_8:Eu$

*Corresponding author. Fax: +31 40 2445619.
E-mail address: h.t.hintzen@tue.nl (H.T. Hintzen).

0022-4596/$ - see front matter © 2007 Elsevier Inc. All rights reserved.
doi:10.1016/j.jssc.2007.11.037

(5 mol%) on structural and luminescence properties as well as on the thermal stability. For an overall comparison, the thermal quenching of $Ba_{1.9}Eu_{0.1}Si_5N_8$ is also included in this work.

2. Experimental

2.1. Starting materials

The binary nitride precursors of SrN_x ($x \approx 0.6$), BaN_x ($x \approx 0.6$) and EuN_x ($x \approx 0.94$) were pre-prepared by a gas–solid reaction. Pure strontium metal (Aldrich, 99.9%, pieces), barium metal (Aldrich, 99.9%, pieces) and Eu metal (CSRE, 99.9%, lumps) were loaded into a molybdenum crucible and heated to 750–800 °C within 360 min in a horizontal tube furnace under purely dried nitrogen and held at this temperature for 8–16 h. Subsequently, the samples were cooled naturally to room temperature. In addition, calcium nitride powder Ca_3N_2 (Alfa, 98%) and α-Si_3N_4 powder (Permascand, P95H, α content 93.2%; oxygen content: ~1.5%) were used as the as-received raw materials.

2.2. Synthesis of undoped and Eu-doped compounds

Undoped-$M_2Si_5N_8$ and Eu-doped $M_2Si_5N_8$ (M = Ca, Sr, Ba) with the composition of $M_{1.9}Eu_{0.1}Si_5N_8$ (M = Ca, Sr, Ba) as well as Eu-doped $(Sr_{1-x}Ca_x)_2Si_5N_8$ with the composition of $Sr_{1.3}Ca_{0.6}Eu_{0.1}Si_5N_8$ were prepared by a solid-state reaction at high temperatures. The Eu concentration is fixed at 5 mol% with respect to the divalent M cations. The Ca_3N_2, SrN_x, BaN_x and EuN_x as well as α-Si_3N_4 starting powders were weighed out, thoroughly mixed and ground together in the appropriate molar ratio in an agate mortar. The powder mixtures were then transferred into molybdenum crucibles. All processes were carried out in a purified-nitrogen-filled glove-box. Subsequently those powder mixtures were heated to 1300–1400 °C with a heating rate of 5 °C/min in a horizontal tube furnace and fired twice at 1300–1400 °C for 12 and 16 h, respectively, under flowing 90%N_2–10%H_2 atmosphere with an intermediate grinding in between. After firing, the samples were cooled down in the furnace.

2.3. X-ray diffraction data collection and structure refinement

All measurements were performed on finely ground samples, which were analysed by X-ray powder diffraction (Rigaku, D/MAX-B) using Cu$K\alpha$ radiation at 40 kV and 30 mA with a graphite monochromator. The phase formation of all samples was checked by a routine scan (2°/min). For structure refinement, X-ray diffraction data were collected from 10° to 120° 2θ at 0.01° intervals, counting for 20 s per step. Structure refinement was carried out by the Rietveld method [14], using the program GSAS [15,16]. The structural parameters of $Ca_2Si_5N_8$ [17] and $Sr_2Si_5N_8$ [18] were used as the initial parameters for structural refinement of $M_{1.9}Eu_{0.1}Si_5N_8$ (M = Ca, Sr) and $Sr_{1.3}Ca_{0.6}Eu_{0.1}Si_5N_8$. Site preferences of Ca^{2+} and Eu^{2+} were examined by manually varying the occupancies of Ca and Eu over two M sites within the stoichiometric constraints.

Based on the refined crystal structures, the MAPLE (Madelung Partial Lattice Energy) value was calculated [19,20]. The coordination polyhedral volume (CPV), polyhedral volume eccentricity (ECCv) and sphericity calculated around M (M = Ca, Sr and/or Eu) and Si were obtained by the program IVTON [21].

2.4. Optical measurements

The diffuse reflection, emission and excitation spectra of the samples were obtained at room temperature by a Perkin Elmer LS 50B spectrophotometer equipped with a Xe flash lamp. The reflection spectra were calibrated with the reflection of black felt (reflection 3%) and white barium sulphate ($BaSO_4$, reflection ~100%) in the wavelength region of 230–700 nm. The excitation and emission slits were set at 5 nm. The emission spectra were corrected by dividing the measured emission intensity by the ratio of the observed spectrum of a calibrated W-lamp and its known spectrum from 300 to 900 nm. Excitation spectra were automatically corrected for the variation in the lamp intensity by a second photomultiplier and a beam-splitter. All the spectra were measured with a scan speed of 100 nm/min. The CIE colour coordinates were calculated from the emission spectra with the excitation wavelength of 450 nm.

The conversion quantum efficiency for $\lambda_{exc} = 465$ nm was determined by dividing the luminescence intensity by the measured absorption along with the corresponding values measured for a standard phosphor (SrS:Eu) with known quantum efficiency. At the same excitation wavelength, the temperature dependence of the quantum efficiency was obtained in the temperature range from 25 to 250 °C with an interval of 50 °C.

3. Results and discussion

3.1. Effect of incorporation of Ca^{2+} on structural characteristics of $Sr_2Si_5N_8$:Eu^{2+}

$Ca_{1.9}Eu_{0.1}Si_5N_8$ and $Sr_{1.9}Eu_{0.1}Si_5N_8$ are obtained as nearly single-phase compounds. For (Sr, Eu)$_2Si_5N_8$ this is as expected, because $Sr_2Si_5N_8$ [18] and $Eu_2Si_5N_8$ [22] are isostructural compounds. For $Ca_{1.9}Eu_{0.1}Si_5N_8$, the selected Eu concentration is below the maximum solubility of Eu (~7 mol%) [3]. Similar to the Ca- and Sr-silicates [11,13], it can be expected that $Ca_2Si_5N_8$ and $Sr_2Si_5N_8$ could also form a limited solid solution due to the fact that $Ca_2Si_5N_8$ [17] and $Sr_2Si_5N_8$ [18] have different crystal structures. For $Sr_{2-x-y}Ca_xEu_ySi_5N_8$, indeed, it was found that only the partial crystalline solid solutions can be formed between $Ca_2Si_5N_8$ and $Sr_2Si_5N_8$ compounds with a maximum

solubility of Ca^{2+} at about $x = 0.6$ in $Sr_2Si_5N_8$ under the present synthetic conditions. When x is greater than $x = 0.6$, impurity phase with unindexed peaks can be obviously observed from the X-ray powder diffraction patterns. For convenient purpose of the structure investigation, we then selected a compound having the maximum solubility of Ca with the composition of $Sr_{1.3}Ca_{0.6}Eu_{0.1}Si_5N_8$ in this work. As a result, incorporation of the Ca^{2+} ions at this level (i.e., $x = 0.6$) is found to form a nearly single-phase $Sr_{1.3}Ca_{0.6}Eu_{0.1}Si_5N_8$ compound just having minor impurity peaks in its X-ray diffraction pattern at about 25.5°, 28.7° and 37.7° in 2θ (Fig. 2). As expected, the lattice parameters of $Sr_{1.3}Ca_{0.6}Eu_{0.1}Si_5N_8$ are smaller than those of $Sr_2Si_5N_8$:Eu^{2+} as a matter of fact that the ionic radius of Ca^{2+} (1.00 Å, CN = 6) is smaller than that of Sr^{2+} (1.18 Å, CN = 6) [23]. Correspondingly, a significant shrinkage of the lattice is observed (Table 1) due to the size effect.

In the $Sr_2Si_5N_8$ lattice, there are two nonequivalent Sr sites, located in a channel along [100] formed by three-dimensional framework of corner-sharing SiN_4 tetrahedra [18]. The two Sr ions are six-fold (Sr(I)–N_6) and seven-fold (Sr(II)–N_7) coordinated with nitrogen atoms [18]. Since the ionic radius of the Eu^{2+} (1.17 Å, CN = 6) ion is similar to that of the Sr^{2+} ion, one can reasonably assume that Eu^{2+} statistically distributes over the two available Sr sites. Indeed, no obvious site preference of Eu^{2+} can be found by the Rietveld refinement not only at low Eu concentration but also at higher Eu concentrations, which is found in our previous work and in agreement with the luminescence properties [3], giving a single symmetric emission band at room temperature. However, one would expect that Ca^{2+}, being much smaller than Sr^{2+}, preferentially occupies the smaller Sr site (i.e., Sr(I)). Initially, the Ca ion was fixed on the Sr(I) and Sr(II) sites with the occupancies of Ca ranging from 1:0 to 0.5:0.5. However, the Rietveld refinement results clearly turned out that these assignments of Ca yield relatively unreasonable structures with the larger R factors, in which some Si–N distances (Si2–N4, Si4–N4) are unusually small (<1.55 Å) in comparison with the normal Si–N distances (1.6–1.9 Å), as found for most nitride and oxynitride compounds [17,18,24]. This suggests that if Ca predominantly occupies the Sr(I) site it would result in a largely distorted structure and eventually makes the whole crystal structure with an orthorhombic lattice be unstable. These distortions in structure can be clearly seen from the calculated ECCv and sphericity [21] on polyhedral Sr(I)N_6 (i.e., 0.3905/0.9547) and Sr(II)N_7 (i.e., 0.2486/0.9898) but also on the framework of tetrahedral SiN_4, in particular, on the Si_4 site (i.e., Si(4)N_4) having a higher ECCv of 0.2634. On the contrary, a relatively reasonable crystal structure, in which all the interatomic distances are in the normal range, can be obtained when the occupancy of Ca on the smaller Sr(I) site is much lower than on the larger Sr(II) site. In addition, this model yields the lower deviated ECCv values of polyhedral Sr(I)N_6 and Sr(II)N_7 as well as tetrahedral SiN_4 in comparison with that in "ideal" $Sr_{1.9}Eu_{0.1}Si_5N_8$ (Tables 1 and 3). Evidently, in this case that Ca preferentially occupies the larger Sr site in $Sr_{1.3}Ca_{0.6}Eu_{0.1}Si_5N_8$ all the Si–N and (Sr, Ca, Eu)–N

Table 1
Crystallographic and luminescence data of $M_{1.9}Eu_{0.1}Si_5N_8$ (M = Ca, Sr) and $Sr_{1.3}Ca_{0.6}Eu_{0.1}Si_5N_8$

Material	$Ca_{1.9}Eu_{0.1}Si_5N_8$	$Sr_{1.9}Eu_{0.1}Si_5N_8$	$Sr_{1.3}Ca_{0.6}Eu_{0.1}Si_5N_8$
Space group	*Monoclinic Cc*	*Orthorhombic Pmn*2_1	*Orthorhombic Pmn*2_1
Lattice parameters			
a (Å)	14.3377(2)	5.7069(1)	5.6966(4)
b (Å)	5.6087(1)	6.8142(1)	6.7864(5)
c (Å)	9.6835(2)	9.3269(1)	9.3161(7)
V (Å^3)	721.52(2)	362.71(1)	360.16(1)
β (°)	112.09(1)		
Z	4	2	2
R_{wp}	0.092	0.082	0.082
R_p	0.059	0.057	0.061
χ^2	2.71	3.80	3.55
Mean M(I)–N[a] (Å) (CPV (Å^3))[b]	2.551±0.284 (15.093±0.038)	2.783±0.148 (16.408±0.285)	2.736±0.169 (15.703±0.527)
Mean M(II)–N[a] (Å) (CPV (Å^3))[b]	2.658±0.227 (20.182±0.033)	2.811±0.159 (18.939±0.521)	2.838±0.183 (17.816±0.851)
Polyhedral volume	0.3834/0.7714 (M(I))	0.2991/0.9799 (M(I))	0.2842/0.9387 (M(I))
Eccentricity/sphericity	0.3006/0.8276 (M(II))	0.2369/0.9686 (M(II))	0.3107/0.9994 (M(II))
Excitation band (nm)	297, 355, 394, 460, 496	294, 334, 395, 463, 505	295, 334, 395, 462, 505
Emission band (nm)	612	620	643
Centre of gravity (cm^{-1})[c]	25 800	26 000	26 100
Crystal-field splitting (cm^{-1})[d]	13 500	14 200	14 100
Stokes shift (cm^{-1})[e]	3800	3700	4300

[a] M(I)–N and M(II)–N: the average distance between M and nitrogen for two M sites.
[b] CPV: coordination polyhedral volume calculated by the program IVTON within a distance of 3.05 Å for M–N.
[c] Centre of gravity calculated from the average energy of the observed 5d excitation levels of Eu^{2+}.
[d] Crystal-field splitting estimated from the energy difference between highest and lowest observed 5d excitation levels of Eu^{2+}.
[e] Stokes shift calculated from the energy difference between the lowest 5d excitation band and emission band of Eu^{2+}.

distances have values in the expected range (Tables 2 and 3). In agreement to our previous work, the Eu^{2+} ions are found to be almost statistically incorporated over the two Sr sites as we observed in the case of $Sr_2Si_5N_8$:Eu^{2+} [3]. Using the refined structures of $Sr_{1.3}Ca_{0.6}Eu_{0.1}Si_5N_8$, the MAPLE values [19,20] were calculated for three structural models based on the distribution of the Ca^{2+} ions: (1) complete on Sr(I); (2) equivalent over Sr(I) and Sr(II); and (3) dominant on Sr(II), i.e., with an occupation fraction above 0.5. The corresponding MAPLE value is about 98 479.3, 98 656.4 and 98 667.3 kJ/mol, respectively, for the proposed models. Owing to the fact that the larger the Madelung part of lattice energy, the more stable the crystal structure, model 3, viz. preference for the Ca ions to occupy the Sr(II) site, is the most probable structure in agreement with the Rietveld refinement results. Furthermore, the MAPLE value of model 3 only shows a smaller different value of 0.4% with the sum of the constitution of binary compounds (i.e., $1.3SrN + 0.2Ca_3N_2 + 0.1EuN + 1.67\alpha\text{-}Si_3N_4$ using the structural data from the ICSD database) which also strongly supports the validity of the structure determination. Fig. 1 shows the refined crystal structure of $Sr_{1.3}Ca_{0.6}Eu_{0.1}Si_5N_8$ and coordination of the Sr(Ca, Eu) atoms with nitrogen atoms. Additionally, the final refinement structural parameters are listed in Tables 1–3.

As mentioned before, $Ca_2Si_5N_8$ and $Sr_2Si_5N_8$ have different crystal structures (Table 1). Therefore, it is understandable that when a large amount of Ca is introduced, due to the size effect, the whole $Sr_2Si_5N_8$

Table 2
Atomic coordinates and isotropic displacement parameters for (a) $Ca_{1.9}Eu_{0.1}Si_5N_8$, (b) $Sr_{1.9}Eu_{0.1}Si_5N_8$ and (c) $Sr_{1.3}Ca_{0.6}Eu_{0.1}Si_5N_8$

Atom	Wyck.	S.O.F.	x/a	y/b	z/c	U (Å^2)
(a)						
(Ca/Eu)1	4*a*	0.96/0.04	−0.042(1)	0.7665(11)	−0.0080(4)	0.01448
(Ca/Eu)2	4*a*	0.94/0.06	0.6085(1)	0.7491(12)	0.1962(1)	0.0129
Si1	4*a*	1.0	0.0573(9)	0.8051(7)	0.3501(13)	0.01252
Si2	4*a*	1.0	0.7521(7)	0.2109(19)	0.3131(10)	0.01199
Si3	4*a*	1.0	0.7517(10)	0.4905(18)	0.0535(12)	0.01122
Si4	4*a*	1.0	0.3599(7)	0.2087(18)	0.3608(10)	0.01369
Si5	4*a*	1.0	0.8517(9)	−0.0029(18)	0.1175(12)	0.01288
N1	4*a*	1.0	0.9847(18)	0.630(4)	0.4245(27)	0.01604
N2	4*a*	1.0	0.1257(19)	−0.0235(33)	0.9769(26)	0.01072
N3	4*a*	1.0	0.7928(10)	0.2489(30)	0.1637(13)	0.01298
N4	4*a*	1.0	0.7994(10)	0.7573(29)	0.1615(14)	0.01048
N5	4*a*	1.0	0.9797(19)	0.9803(31)	0.2036(27)	0.01276
N6	4*a*	1.0	0.8287(10)	0.0058(21)	0.9297(16)	0.01106
N7	4*a*	1.0	0.6255(16)	0.1616(32)	0.2622(24)	0.00326
N8	4*a*	1.0	0.7960(11)	0.4917(24)	0.4065(17)	0.01051
(b)						
(Sr/Eu)1	2*a*	0.95/0.05	0	0.8708(4)	−0.0014(1)	0.01392
(Sr/Eu)2	2*a*	0.95/0.05	0	0.8790(4)	0.3665	0.01415
Si1	4*b*	1.0	0.2525(3)	0.6646(3)	0.6816(12)	0.01311
Si2	2*a*	1.0	0	0.0552(4)	0.6716(8)	0.01293
Si3	2*a*	1.0	0	0.4165(13)	0.4562(10)	0.0129
Si4	2*a*	1.0	0	0.4103(13)	0.8986(9)	0.01145
N1	2*a*	1.0	0	0.1975(25)	0.5234(28)	0.01275
N2	4*b*	1.0	0.2466(7)	0.9063(7)	0.6856(19)	0.01416
N3	4*b*	1.0	0.2496(10)	0.4523(9)	0.0083(8)	0.01196
N4	2*a*	1.0	0	0.5820(12)	0.7693(8)	0.01309
N5	2*a*	1.0	0	0.1773(24)	0.8444(27)	0.00426
N6	2*a*	1.0	0	0.4226(11)	0.2619(9)	0.00647
(c)						
(Sr/Ca/Eu)1	2*a*	0.86/0.1/0.05	0.0	0.8747(3)	0.0015(2)	0.02811
(Sr/Ca/Eu)2	2*a*	0.44/0.5/0.05	0.0	0.8822(3)	0.3677(1)	0.00699
Si1	4*b*	1.0	0.2529(4)	0.6671(2)	0.6844(6)	0.01072
Si2	2*a*	1.0	0.0	0.0570(3)	0.6727(6)	0.00659
Si3	2*a*	1.0	0.0	0.4219(8)	0.4641(7)	0.00748
Si4	2*a*	1.0	0.0	0.4033(8)	0.9051(7)	0.01461
N1	2*a*	1.0	0.0	0.1874(2)	0.5255(2)	0.00542
N2	4*b*	1.0	0.2494(7)	0.9064(6)	0.6708(9)	0.01052
N3	4*b*	1.0	0.2513(9)	0.4549(8)	0.0201(8)	0.01499
N4	2*a*	1.0	0.0	0.5835(11)	0.7748(8)	0.01101
N5	2*a*	1.0	0.0	0.1783(22)	0.8388(19)	0.00698
N6	2*a*	1.0	0.0	0.4239(10)	0.2677(9)	0.00035

Table 3
Selected interatomic distances (Å) and calculated polyhedral volume eccentricity (ECCv) of SiN_4 for (a) $Ca_{1.9}Eu_{0.1}Si_5N_8$, $M=$(Ca, Eu) (b) $Sr_{1.9}Eu_{0.1}Si_5N_8$, $M=$(Sr, Eu) and (c) $Sr_{1.3}Ca_{0.6}Eu_{0.1}Si_5N_8$, $M=$(Sr,Ca,Eu)

(a)			
M1–N2	2.254(26)	Si1–N7	1.718(21)
M1–N1	2.305(21)	Si1–N5	1.741(23)
M1–N5	2.459(22)	Si1–N2	1.750(20)
M1–N6	2.612(13)	Si1–N1	1.770(23)
M1–N7	2.644(22)	Mean Si1–N	1.745(22)
M1–N8	3.034(13)	ECCv	0.0505
M1–N5	3.063(22)		
		Si2–N7	1.716(21)
M2–N7	2.388(19)	Si2–N6	1.739(15)
M2–N5	2.406(23)	Si2–N3	1.765(12)
M2–N1	2.650(25)	Si2–N8	1.808(18)
M2–N2	2.703(22)	Mean Si1–N	1.757(14)
M2–N4	2.880(12)	ECCv	0.0956
M2–N2	2.922(23)		
M2–N8	3.056(14)	Si3–N2	1.676(22)
		Si3–N3	1.688(18)
		Si3–N8	1.767(16)
		Si3–N4	1.806(17)
		Mean Si1–N	1.734(18)
		ECCv	0.1471
		Si4–N8	1.680(16)
		Si4–N1	1.718(24)
		Si4–N4	1.814(13)
		Si4–N6	1.853(15)
		Mean Si1–N	1.766(17)
		ECCv	0.1864
		Si5–N4	1.672(18)
		Si5–N5	1.709(22)
		Si5–N6	1.723(15)
		Si5–N3	1.786(18)
		Mean Si1–N	1.722(18)
		ECCv	0.1213
(b)			
M1–N5	2.536(18)	Si1–N2	1.648(5)
M1–N2	2.728(12) × 2	Si1–N6	1.705(6)
M1–N1	2.900(2) × 2	Si1–N3	1.750(6)
M1–N4	2.906(8)	Si1–N4	1.802(9)
		Mean Si1–N	1.726(7)
M2–N1	2.617(19)	ECCv	0.1559
M2–N2	2.661(12) × 2		
M2–N5	2.887(3) × 2	Si2–N1	1.689(25)
M2–N3	2.981(7) × 2	Si2–N2	1.740(5) × 2
		Si2–N5	1.814(25)
		Mean Si2–N	1.745(15)
		ECCv	0.1300
		Si3–N1	1.618(19)
		Si3–N3	1.755(7) × 2
		Si3–N6	1.812(10)
		Mean Si3–N	1.735(11)
		ECCv	0.1948
		Si4–N5	1.666(18)
		Si4–N4	1.681(11)
		Si4–N3	1.777(7) × 2
		Mean Si4–N	1.725(11)
		ECCv	0.1523
(c)			
M1–N5	2.558(16)	Si1–N2	1.629(5)
M1–N2	2.595(6) × 2	Si1–N6	1.722(4)
M1–N1	2.888(3) × 2	Si1–N3	1.740(7)
M1–N4	2.892(7)	Si1–N4	1.762(4)
		Mean Si1–N	1.713(5)
M2–N1	2.540(15)	ECCv	0.1438
M2–N2	2.731(7) × 2		
M2–N5	2.890(3) × 2	Si2–N1	1.632(18)
M2–N3	3.042(6) × 2	Si2–N2	1.750(4) × 2
		Si2–N5	1.753(18)
		Mean Si1–N	1.721(11)
		ECCv	0.1469
		Si3–N1	1.691(13)
		Si3–N3	1.726(5) × 2
		Si3–N6	1.830(8)
		Mean Si1–N	1.743(8)
		ECCv	0.1462
		Si4–N5	1.647(14)
		Si4–N4	1.723(9)
		Si4–N3	1.822(6) × 2
		Mean Si1–N	1.754(9)
		ECCv	0.1977

lattice has to adapt itself to counteract the overall contraction originating from the replacement of Sr^{2+} by Ca^{2+}. If Ca preferentially occupies the smallest Sr(I) site, the (Sr, Ca, Eu)(I)–N distances will become too much smaller in partial than the (Sr, Ca, Eu)(II)–N distances resulting in marked structural distortion in agreement with the calculated ECCv data. Obviously, in this way, it will eventually result in a higher lattice stress which is not in favour of the stability of the crystal structure. In contrast, the proposed structure (Table 2) leads to the normal bond lengths of Si–N (Table 3) and the highest MAPLE value as well. Fig. 2 shows the refined X-ray diffraction patterns of $Sr_{1.9}Eu_{0.1}Si_5N_8$ and $Sr_{1.3}Ca_{0.6}Eu_{0.1}Si_5N_8$, demonstrating that the observed X-ray diffraction patterns are in fair agreement with that of the calculated ones.

3.2. Effect of incorporation of Ca^{2+} on the luminescence properties of $Sr_2Si_5N_8$:Eu^2

Similar to $Sr_2Si_5N_8$:Eu^{2+}, the diffuse reflection spectrum of $Sr_{1.3}Ca_{0.6}Eu_{0.1}Si_5N_8$ has two absorption bands of Eu^{2+} centred at about 300 and 425 nm, as shown in Fig. 3. With incorporation of Ca the reflection in the spectral range of 400–465 nm decreases with about 5% for $Sr_{1.3}Ca_{0.6}Eu_{0.1}Si_5N_8$ as compared to $Sr_{1.9}Eu_{0.1}Si_5N_8$, showing the same tendency as an increase of Eu concentration to enhance the absorption [3]. Herein, it is worth noting that the percentage of EuN_x ($x\approx0.94$) by weight in composition is higher in $Sr_{1.3}Ca_{0.6}Eu_{0.1}Si_5N_8$ than in $Sr_{1.9}Eu_{0.1}Si_5N_8$, namely 4.1 wt% vs. 3.8 wt%, although the molar percentage is the same (5 mol%) with respect to (Sr, Ca) and Sr. Therefore, an increase of Eu content by weight should also have some effects not only on the reflection spectrum but also on the PL luminescence spectra.

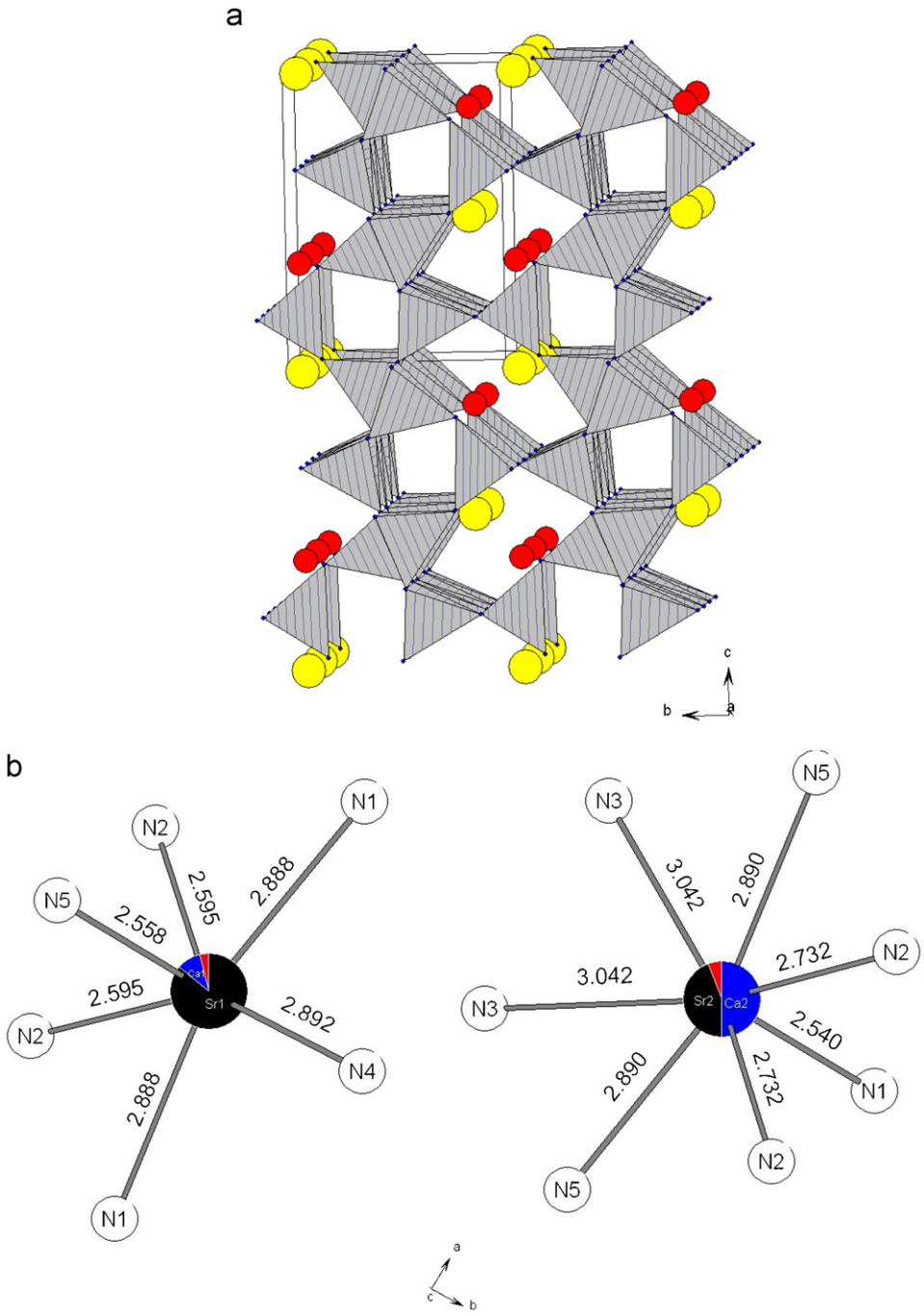

Fig. 1. (a) Crystal structure, view along [100], the large and small spheres represent Sr and Ca dominant sites, respectively; (b) coordination of the Sr(Ca, Eu) atoms (black sphere) and the Sr(Ca, Eu)–N distances (Å) in $Sr_{1.3}Ca_{0.6}Eu_{0.1}Si_5N_8$.

Fig. 4 shows the excitation and emission spectra of $Sr_{1.3}Ca_{0.6}Eu_{0.1}Si_5N_8$ and $Sr_{1.9}Eu_{0.1}Si_5N_8$. Because of lack of sharp emission lines of Eu^{3+} in the emission spectra at room temperature, both the excitation and emission bands are originated from the $4f^65d^1 \rightarrow 4f^7$ transition of Eu^{2+}. Five Eu^{2+} excitation bands at about 295, 334, 395, 462, 505 nm can be discriminated. The excitation band peaking at about 250 nm is attributed to host lattice excitation by the valence band to the conduction band transitions at around the absorption edge of the host lattice (Fig. 3). Obviously, the partial replacement of Sr by Ca also does not significantly change the position of the excitation bands of $Sr_{1.9}Eu_{0.1}Si_5N_8$ (Fig. 4). This further verifies our previous conclusion that the excitation characteristics of Eu^{2+}-doped $M_2Si_5N_8$ are almost independent of the type of M (M = Ca, Sr, Ba) [3]. Whereas, the maximum of the emission band of Eu^{2+} significantly shifts to long wavelength from 620 to 643 nm as the Ca^{2+} ion is incorporated into the parent $Sr_2Si_5N_8$ lattice (Fig. 4). As a result, the corresponding colour coordinates (CIE 1931 chromaticity), very similar to the effect of the Eu concentration on the luminescence properties of

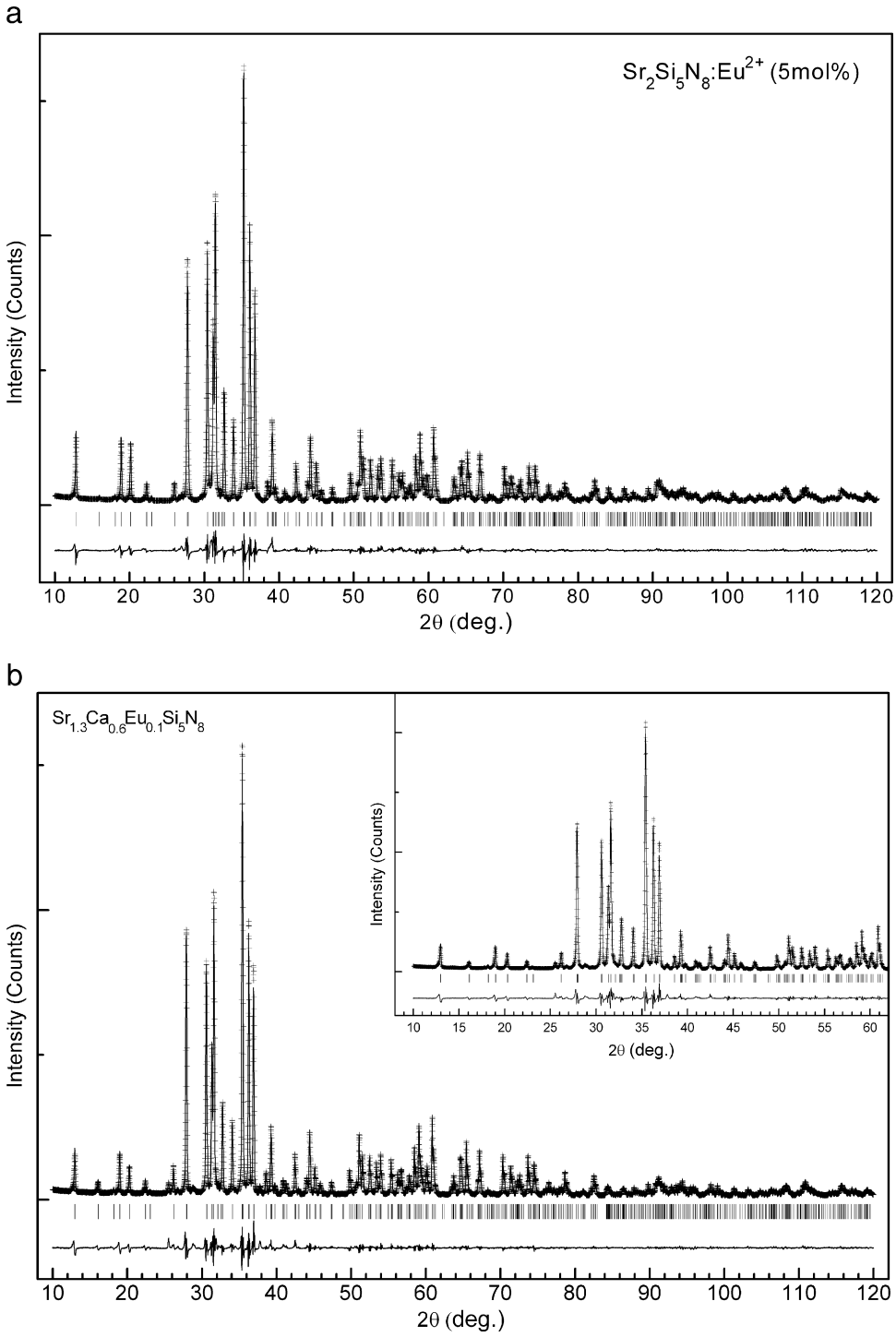

Fig. 2. Observed (+), calculated (solid) X-ray powder diffraction patterns and the difference profile of the Rietveld refinement of (a) $Sr_{1.9}Eu_{0.1}Si_5N_8$ and (b) $Sr_{1.3}Ca_{0.6}Eu_{0.1}Si_5N_8$.

Eu^{2+}-doped $Sr_2Si_5N_8$, also have been changed from (0.63, 0.37) to (0.65, 0.35), extending to the deep red region. The centre of gravity (the average energies of the observed 5*d* excitation bands) of Eu^{2+} is roughly calculated, and the crystal-field splitting (the energy difference between highest and lowest observed 5*d* excitation bands of Eu^{2+}) in $Sr_{1.9}Eu_{0.1}Si_5N_8$ and $Sr_{1.3}Ca_{0.6}Eu_{0.1}Si_5N_8$ is estimated from the obtained excitation spectra, as shown in Table 1. In general, the position of the Eu^{2+} emission band mainly depends on the effects of the covalency (i.e., nephelauxetic effect) and the crystal-field splitting of the 5*d* levels of Eu^{2+} as well as the Stokes shift. From Table 1, it is clear that the changes of the centre of gravity of the 5*d* excitation bands of Eu^{2+} and the crystal-field splitting of the 5*d* levels of Eu^{2+} are so small for the case with and without Ca substitution, indicating that the effect of Ca substitution on

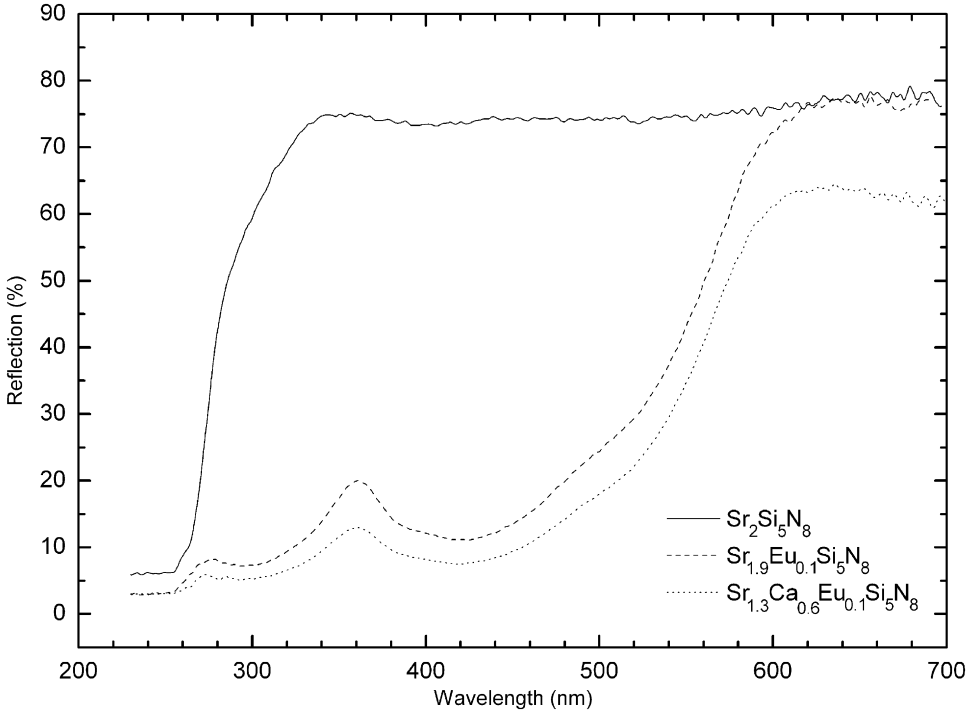

Fig. 3. Diffuse reflection spectra of $Sr_2Si_5N_8$, $Sr_{1.9}Eu_{0.1}Si_5N_8$ and $Sr_{1.3}Ca_{0.6}Eu_{0.1}Si_5N_8$.

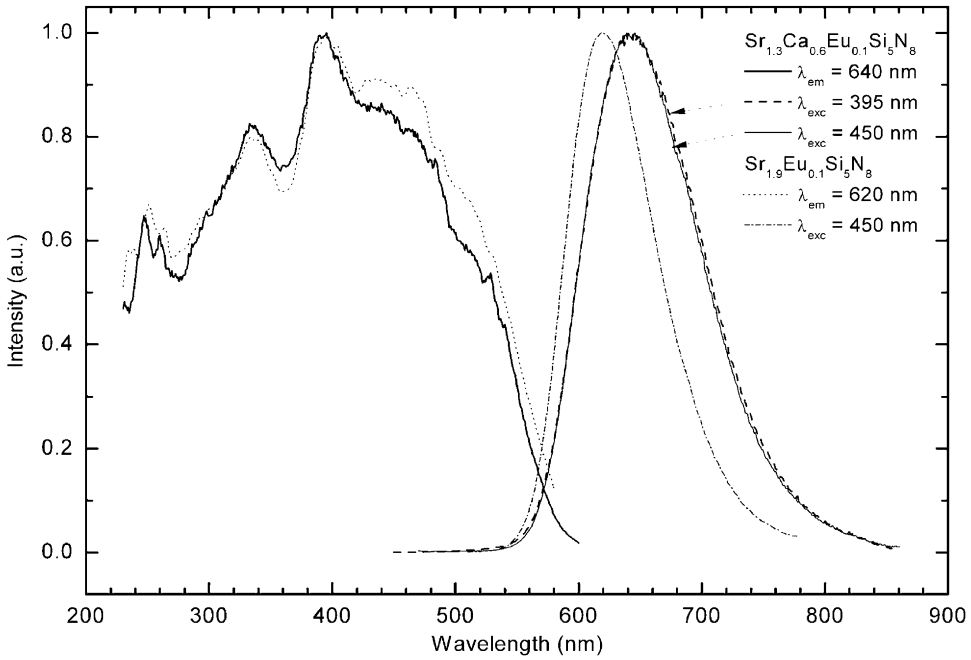

Fig. 4. Excitation (left) and emission (right) spectra of $Sr_{1.9}Eu_{0.1}Si_5N_8$ ($\lambda_{exc} = 450$ nm, $\lambda_{em} = 620$ nm) and $Sr_{1.3}Ca_{0.6}Eu_{0.1}Si_5N_8$ ($\lambda_{exc} = 395$, 450 nm, $\lambda_{em} = 640$ nm).

the covalency and the crystal-field strength around the Eu^{2+} ions is only very small (Table 1). Thus, based on the fact that the larger Stokes shift leads to the larger red-shift, one of the possible reasons for the red-shift of the Eu^{2+} emission band could be from an increase of the Stokes shift, which probably can be explained by the shrinkage of the Sr sites as Ca is incorporated, especially for the larger Sr(II) site due to preferential Ca substitution on it. The changes in the local structures around the Sr sites can be characterized by the following crystallographic parameters, i.e., the CPV and the ECCv. First, the CPV values of the (Sr, Ca, Eu)N(n) polyhedron ($n = 6$, 7, respectively, within a distance of 0–3.05 Å for the (Sr, Ca, Eu)–N bonds) show marked decrease after incorporation of the Ca ions in

$Sr_{1.9}Eu_{0.1}Si_5N_8$. Second, the ECCv value on the larger Sr(II) site is also significantly increased by about 31% (Table 1). In an isotypic lattice, on a smaller crystallographic site a larger Stokes shift of the Eu^{2+} luminescence is expected due to a large relaxation of 5*d* electron from its excitation states, thus resulting in a longer emission wavelength. This observation is in agreement with a number of previous investigations where such a relationship is established between the Stokes shift and the site size [10,25,26]. One of the possible reasons for that is the relaxation in the excited state of Eu^{2+} becoming promoted when the size of the alkaline earth ion decreases [25]. In addition, given a higher ECCv value (i.e., a larger distortion) on the (Sr, Ca, Eu)(II) site in $Sr_{1.3}Ca_{0.6}Eu_{0.1}Si_5N_8$, it is expected that the emission band must be shifted because the position of the emission band strongly depends on the local symmetry around the Eu coordination as well [10]. Further, the red-shift of the emission band of Eu^{2+} could also form an increased possibility of the energy transfer between the Eu^{2+} ions caused by a decrease of the shortest distances between two Eu ions, i.e., 3.4123 Å for (Sr, Ca, Eu)1–(Sr, Ca, Eu)2 and 3.4322 Å for (Sr, Eu)1–(Sr, Eu)2 in $Sr_{1.3}Ca_{0.6}Eu_{0.1}Si_5N_8$ and $Sr_{1.9}Eu_{0.1}Si_5N_8$ unit cells, respectively, and an increase of the Eu content (0.3 wt%) by weight in composition of $Sr_{1.3}Ca_{0.6}Eu_{0.1}Si_5N_8$ as described above.

Fig. 5 shows the temperature dependence of $M_{1.9}Eu_{0.1}Si_5N_8$ (M = Ca, Sr, Ba) and $Sr_{1.3}Ca_{0.6}Eu_{0.1}Si_5N_8$ under excitation at 465 nm. The thermal quenching rate is observed to decrease in the sequence of Sr > (Sr,Ca) > Ba > Ca, corresponding to the quenching temperatures ($T_{1/2}$: the temperature with half the initial emission intensity at room temperature) at about ~300, 233, 220 and 130 °C, respectively. Due to a lower quenching temperature (~130 °C), $Ca_{0.9}Eu_{0.1}Si_5N_8$ alone is not a good phosphor for use in white-light LEDs. Nevertheless, the conversion efficiency (λ_{exc} = 465 nm) of not optimized

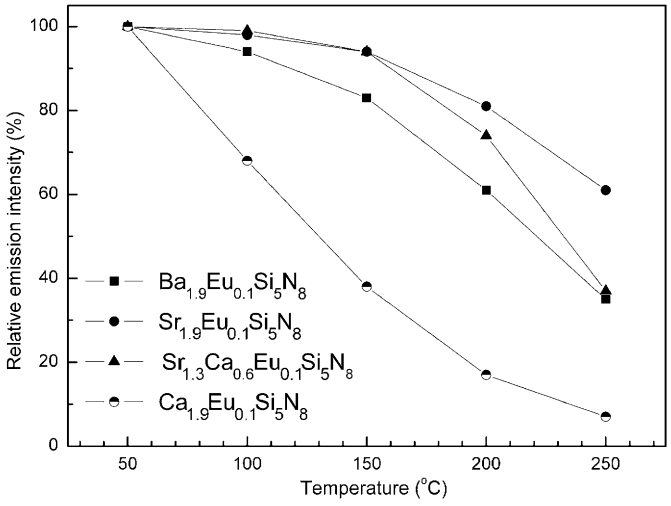

Fig. 5. The temperature dependence of the luminescence efficiency of $M_{1.9}Eu_{0.1}Si_5N_8$ (M = Ca, Sr, Ba) and $Sr_{1.3}Ca_{0.6}Eu_{0.1}Si_5N_8$ (λ_{exc} = 465 nm).

$Sr_{1.3}Ca_{0.6}Eu_{0.1}Si_5N_8$ (~73%) is only slightly lower as compared to $Sr_{1.9}Eu_{0.1}Si_5N_8$ (~80%) at room temperature. Therefore, by incorporation of Ca the emission wavelength can be tailored, while keeping the conversion efficiency at about the same level. Below 150 °C the thermal quenching rate of $Sr_{1.3}Ca_{0.6}Eu_{0.1}Si_5N_8$ is similar to that of $Sr_{1.9}Eu_{0.1}Si_5N_8$, but above 150 °C it significantly increases (Fig. 5) as expected from its larger Stokes shift (Table 1). Moreover, it is expected that the conversion efficiency and thermal quenching behaviour of $Sr_{2-x-y}Ca_xEu_ySi_5N_8$ can be further increased by optimization of the Ca and Eu concentrations enabling competitive red-emitting LED conversion phosphors whose emission band maximum can be varied by adjustment of the Ca content.

3.3. Conclusions

The incorporation of Ca has some influence on the structural and luminescence properties of $Sr_2Si_5N_8:Eu^{2+}$. The Rietveld refinement of X-ray powder diffraction data shows that the Ca^{2+} ions preferentially occupy a larger crystallographic Sr site in agreement with the MAPLE calculations, while the Eu^{2+} ions statistically distribute over the two available Sr sites in the $Sr_2Si_5N_8$ and $(Sr, Ca)_2Si_5N_8$ lattices. In addition, the replacement of Sr by Ca in $Sr_2Si_5N_8:Eu^{2+}$ results in a significant red-shift of the emission band maximum from about 620 to 643 nm, while the absorption, the conversion efficiency and the thermal quenching behaviour for 465 nm excitation almost remain similar.

Acknowledgments

We would like to thank Dr. Detlef Starick and Ms. Sylke Rösler of Leuchtstoffwerk Breitungen GmbH (Germany) for the temperature dependent quantum efficiency measurements. We are indebted to Dr. Tonci Balic-Zunic of Geological Institute, University of Copenhagen (Denmark) for kindly providing us the program of IVTON.

References

[1] H.T. Hintzen, J.W.H. van Krevel, G. Botty, EP 1104 799 A1, 1999.
[2] J.W.H. van Krevel, Ph.D. Thesis, Eindhoven University of Technology, 2000.
[3] Y.Q. Li, J.E.J. van Steen, A.C.A. Delsing, F.J. D lvo, G. de With, H.T. Hintzen, J. Alloys Compd. 417 (2006) 273.
[4] R.B. Mueller-Mach, G.O. Mueller, M.R. Krames, H.A. Höppe, F. Stadler, W. Schnick, T. Jüestel, P. Schmidt, Phys. Stat. Sol. (a) 202 (2005) 1727.
[5] X. Piao, T. Horikawa, H. Hanzawa, K. Machida, J. Electrochem. Soc. 153 (2006) H232.
[6] L.S. Rohwer, A.M. Srivastava, The Electrochemical Society Interface, 2003, p. 36.
[7] R.B. Muller-Mach, G.O. Mueller, T. Jüestel, P. Schmidt, US 6680569 B2, 2004.
[8] H.A. Höppe, H. Lutz, P. Morys, W. Schnick, A. Seilmeier, J. Phys. Chem. Solids 61 (2000) 2001.

[9] J.Y. Taso (Ed.), Light Emitting Diodes (LEDs) for General Illumination Update 2002, Optoelectronics Industry Development Association, Washington, DC, 2002.
[10] G. Blasse, B.C. Grabmaier, Luminescent Materials, Springer, Berlin, 1994.
[11] T.L. Barry, J. Electrochem. Soc. 115 (1968) 1181.
[12] K. Kato, F. Okamoto, Jpn. J. Appl. Phys. 22 (1983) 76.
[13] H. Kasano, K. Megumi, H. Yamamoto, J. Electrochem. Soc. 131 (1984) 1954.
[14] H.M. Rietveld, J. Appl. Crystallogr. 2 (1969) 65.
[15] A.C. Larson, R.B. Von Dreele, Report LAUR 86-748, Los Alamos National Laboratory, Los Alamos, NM, 2000.
[16] B.H. Toby, J. Appl. Crystallogr. 34 (2001) 210.
[17] T. Schlieper, W. Milius, W. Schnick, Z. Anorg. Allg. Chem. 621 (1995) 1380.
[18] T. Schlieper, W. Schnick, Z. Anorg. Allg. Chem. 621 (1995) 1037.
[19] R. Hoppe, Angew. Chem. 78 (1966) 52.
[20] R. Hoppe, Angew. Chem. 82 (1970) 7.
[21] T. Balic Zunic, I. Vickovic, J. Appl. Crystallogr. 29 (1996) 305.
[22] H. Huppertz, W. Schnick, Acta Crystallogr. C 53 (1997) 1751.
[23] R.D. Shannon, Acta Crystallogr. A 32 (1976) 751.
[24] W. Schnick, H. Huppertz, Chem. Eur. J. 3 (1997) 679.
[25] A. Meijerink, G. Blasse, J. Lumin. 43 (1989) 283.
[26] Y.Q. Li, C.M. Fang, G. de With, H.T. Hintzen, J. Solid State Chem. 177 (2004) 4687.